coatings

MDPI

Article

Extreme High-Speed DED of AISI M2 Steel for Coating Application and Additive Manufacturing

Min-Uh Ko [1,*], Julius Cüppers [2], Thomas Schopphoven [1] and Constantin Häfner [1,3]

[1] Fraunhofer Institute for Lasertechnology ILT, 52074 Aachen, Germany; thomas.schopphoven@ilt.fraunhofer.de (T.S.); constantin.haefner@ilt.fraunhofer.de (C.H.)
[2] Makino Asia Pte Ltd., Singapore 629649, Singapore; julius.cueppers@makino.com.sg
[3] Chair for Lasertechnology LLT, RWTH Aachen University, 52074 Aachen, Germany
* Correspondence: min-uh.ko@ilt.fraunhofer.de; Tel.: +49-241-8906-8441

Abstract: This work focuses on the development of the 3D Extreme High-Speed DED process (EHLA3D), a variant of the laser-based Directed Energy Deposition (DED-LB), for the processing of the material HSS M2. Characteristics for the EHLA3D process are feed rates of >20 m/min, high cooling rates, and layer thicknesses in the range of 100 µm. This work covers the three subsequent stages: (1) a process parameter study on single-track deposition, (2) development of coating parameters, and (3) development of parameters for AM. In scope of stage 2, a coating parameter with a powder mass flow of $\dot{m}$ = 1.9 kg/h was achieved. A variation in the deposition angles indicates that the coating process is feasible within a tilted deviation of up to 20°. In stage 3, a process parameter with a deposition rate of $\dot{m}$ = 0.4 kg/h was developed. The hardness results of the as-built specimen with 67 HRC exceeds the hardness of conventionally manufactured and heat-treated M2 steel. The results of this work indicate that the EHLA3D process can be potentially utilized for the additive manufacturing with the material M2 as well as for the productive deposition of anti-wear coatings on free-form surfaces.

Keywords: directed energy deposition (DED); extreme high-speed directed energy deposition (EHLA); EHLA3D; laser metal deposition (LMD); HSS M2; 1.3343; additive manufacturing; anti-wear coating; hardfacing; wear resistance

Citation: Ko, M.-U.; Cüppers, J.; Schopphoven, T.; Häfner, C. Extreme High-Speed DED of AISI M2 Steel for Coating Application and Additive Manufacturing. *Coatings* **2024**, *14*, 953. https://doi.org/10.3390/coatings14080953

Academic Editor: Chi Wai Chan

Received: 20 June 2024
Revised: 22 July 2024
Accepted: 24 July 2024
Published: 31 July 2024

1. Introduction and State-of-the-Art

In the laser-based Directed Energy Deposition (DED-LB) process, a laser beam melts a metallic surface while a metallic additive material, either in the form of powder or a wire, is added to the melt pool. The additive material is molten in the melt pool and after solidification a weld bead is deposited. This process principle allows for the utilization of the DED-LB technology as a flexible process for repair, cladding, and additive manufacturing of metallic components [1,2]. As such, an active research field is the deposition of hardfacing materials as anti-wear coatings via DED-LB. Among potential materials, due to the high hardness and good anti-wear properties, AISI M2 high-speed steel has been investigated in several studies for application as a DED-LB hardfacing material [3–5].

Conventionally, M2 is used as one of the most common high-speed tool steels for cutting and milling tools. Its properties of a high hardness ~66 HRC and overall good toughness is based on a high carbon content of up to 0.88 wt.% and the main alloying elements Mo, V, and W, resulting in the precipitation of carbides in a martensitic matrix [6–8]. To achieve the final operating properties of conventionally manufactured M2, a heat treatment is required, which typically involves the steps of annealing, hardening, and tempering [9].

According to studies regarding the deposition of M2 powder via DED-LB, a heat treatment is not required as the resulting hardness of the coating in the as-built condition is

comparable to conventionally manufactured M2 after heat treatment. Defect free layers with a thickness of up to 2 mm can be deposited when using a beam power of P = 900 W, powder mass flow $\dot{m}$ = 0.3 kg/h, and a feed rate of v_f = 0.85 m/min [3,4].

Potentially, 3D structures can also be manufactured when using the Laser Powder Bed Fusion (LPBF) process. However, due to the low weldability of M2 caused by the high carbon content, an in situ pre-heating of the substrate plate at >200 °C is required for a defect free specimen [10].

In this study, the processability of M2 for anti-wear coating and additive manufacturing was investigated with a modified variant of DED-LB called Extreme High-Speed Directed Energy Deposition (German acronym—EHLA). The EHLA process was introduced by Fraunhofer ILT and is based on the positioning of the powder jet focus above the melt pool (see Figure 1). Through this modification, the powder particles are molten in flight as most of the beam radiation is absorbed by the powder gas jet, enabling process feed rates of up to 200 m/min [11]. As a comparison, usual DED-LB feed rates are in the range of 1 m/min since solid powder particles are added to the melt pool and require a dwelling time for liquification.

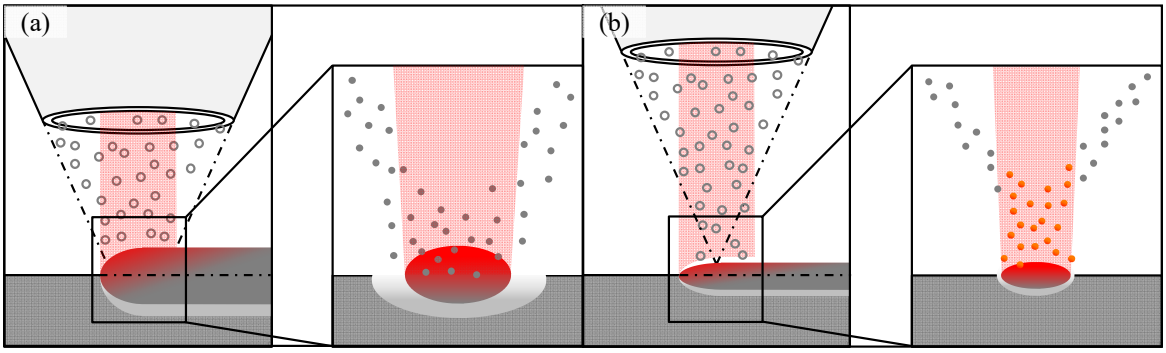

Figure 1. Comparison between process set-ups: (**a**) conventional DED-LB and (**b**) EHLA [11].

Furthermore, since most of the beam energy is absorbed by the powder gas jet, a smaller heat input is generated on the processing surface which results in smaller dimensions of the melt pool and heat-affected zones. In combination with a rapid cooling rate, which is comparable to the LPBF process and adjustable with the feed rate used, the processability of difficult-to-weld materials can be improved when compared to the conventional DED-LB process [12–14]. Due to the process benefits, EHLA technology has been successfully transferred to the industry as an efficient anti-wear and -corrosion coating process [15]. However, as EHLA systems are lathe-type machines, the applications are mostly limited to rotational symmetric components like cylinders, disks, and shafts as the feed rates are realized via the rotation of the component (see Figure 2).

Figure 2. EHLA coating process of a brake disk.

To utilize the EHLA process for free-form surfaces and additive manufacturing application, high-speed operation in three dimensions is required and hence the term EHLA3D is introduced. The transfer from rotational, mostly 2D application to 3D application involves

the prerequisite of machine systems capable of reliable operation with lateral feed rates of v_f > 20 m/min. The EHLA technology was successfully transferred and demonstrated on a parallel kinematic system from ponticon GmbH [16,17] and on a modified five-axis CNC-type machine from Makino Asia Pte Ltd., Singapore. [18]. So far, EHLA3D processes were demonstrated with the materials 316L stainless steel [19] and IN718 [20]. In the case of 316L stainless steel and compared to conventional DED-LB, the EHLA3D process resulted in a finer microstructure, which increased the yield strength by 100 MPa [19]. For IN718, the feasibility of depositing thin-walled structures with a thickness of ~400 µm with a powder mass flow of $\dot{m}$ = 15 g/min was demonstrated [20]. However, due to the limited and recent availability of the EHLA3D machine systems, the feasible process parameter windows for additional materials need to be further investigated. As the EHLA technology combines high productivity with a low heat input, the process can potentially improve the productivity and processability of M2 deposition for the anti-wear coating application for free-form surfaces. Furthermore, as an additive manufacturing technology, the EHLA3D process potentially utilizes the deposition of 3D structures and volumes with M2.

2. Materials and Methods

2.1. System Technology

All experiments were conducted on a modified 5-axis CNC prototype machine developed by Makino Asia Pte Ltd., Singapore. (see Figure 3). The machine can operate the processing optics with a maximum feed rate of v_f = 30 m/min in x-y-z and is equipped with a turn/tilt table for B + C axis rotation. The optical set-up consists of a Beo D70 processing optics from Trumpf GmbH and is combined with a LDF4000-8 beam source from Laserline GmbH. The laser focus diameter of d_{focus} = 400 µm results from an optical aspect ratio of 2:1 and a laser fiber core diameter of d_{fiber} = 200 µm, and the beam parameter product of BPP = 8 mm mrad. The beam diameter used for the process can be set up by the motorized collimation system of the processing optics. The powder nozzle is a Highno. 4.0 from HD Sonderoptiken and is specified with a stand-off distance of 9 mm.

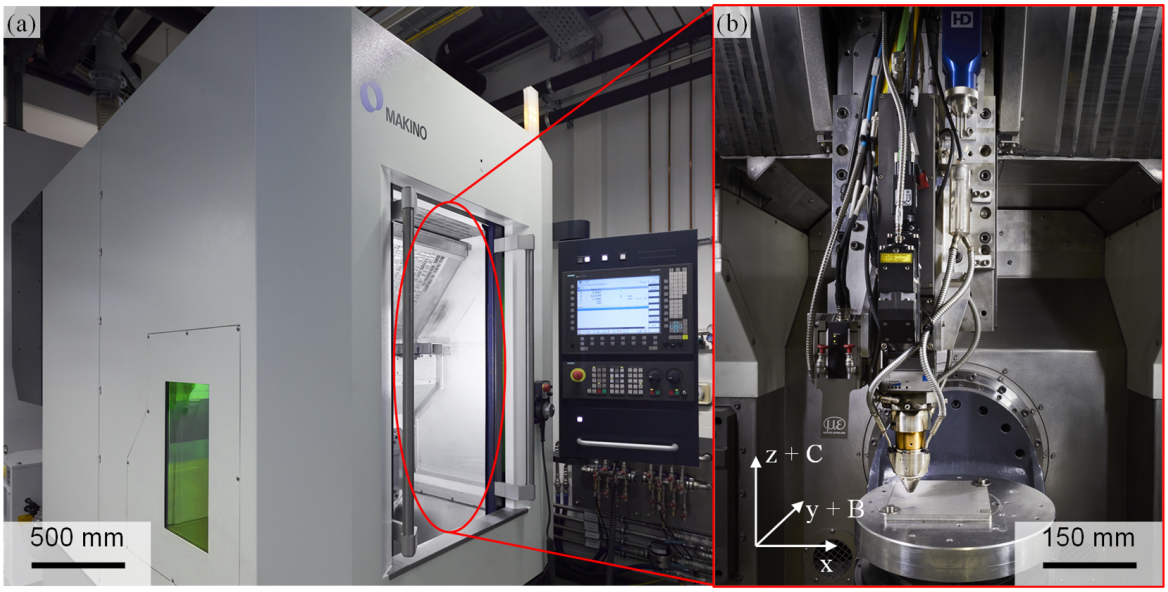

Figure 3. System technology, (**a**) High-speed 5-axis CNC prototype and (**b**) machining area with Trumpf Beo D70 processing optics.

2.2. Materials

The additive material used for this work is M2 powder procured from Eckart TLS GmbH. The powder is specified with a powder particle distribution between 15 and 45 µm.

The powder material as well as the substrate plates with a thickness of 10 mm have the same chemical composition (see Table 1).

Table 1. Chemical composition of the powder and substrate material.

[wt.%]					
C	**Si max.**	**Cr**	**Mo**	**V**	**W**
0.86–0.94	0.45	3.8–4.5	4.7–5.2	1.7–2.1	5.9–6.7

Before the deposition, the surface of the substrate plates were cleaned with Ethanol. No further pre-treatment of the substrates was applied.

2.3. Methods

2.3.1. Single-Track Evaluation

To assess the initial dependencies between process parameter and deposition outcome with the material M2, a parameter study on single-track deposition was conducted in a first stage. The variated process parameters are presented in Table 2. The feed rate was kept constant at v_f = 30 m/min for all experiments.

Table 2. Process parameter for single-track evaluation.

Beam Diameter [mm]	Beam Power [W]	Powder Mass Flow [kg/h]	Carrier Gas Flow [l/min]	Feed Rate [m/min]
1.4	2800	2.2	8	30
1.5				
1.6	1800–3000	0.4–2.2	6; 8	
1.7	2800	2.2	8	
1.8				

Every deposited single track had a length of l_{bead} = 30 mm and was evaluated via metallographic cross-sections at the beginning, middle, and end position of the track. Evaluation criteria of the single tracks are the following (see Figure 4):

- Weld bead width;
- Weld bead height;
- Deposition area;
- Dilution zone area.

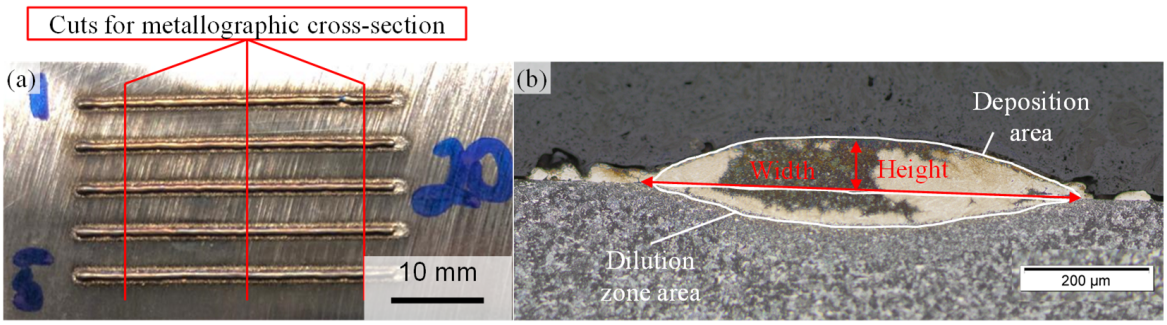

Figure 4. (**a**) Deposited single tracks with indication of the positions for metallographic cross-sections. (**b**) Example of a single-track metallographic cross-section with evaluation criteria.

After the parameter study, two parameter sets are selected for the transfer to a coating process. By selecting two process parameter sets, the respective approaches for a high

productivity (high powder mass flow/high beam power) process and a process with low heat input (low powder mass flow/low beam power) are investigated. For the transfer, the parameters which resulted in the following single-track deposition criteria were selected:

- No bonding defects;
  - Depth of dilution zone: 20–50 µm;
- No pores;
- No crack formation;
- Set powder mass flow:
  - High productivity: 1.9 kg/h;
  - Low heat input: 0.4 kg/h.

2.3.2. Coating Deposition

In the second stage, the selected process parameters were used to develop a single-layer coating process via the deposition of multiple, overlapping weld beads. The influence of the overlap on the resulting coating was investigated via variation in the hatching parameter h (see Figure 5).

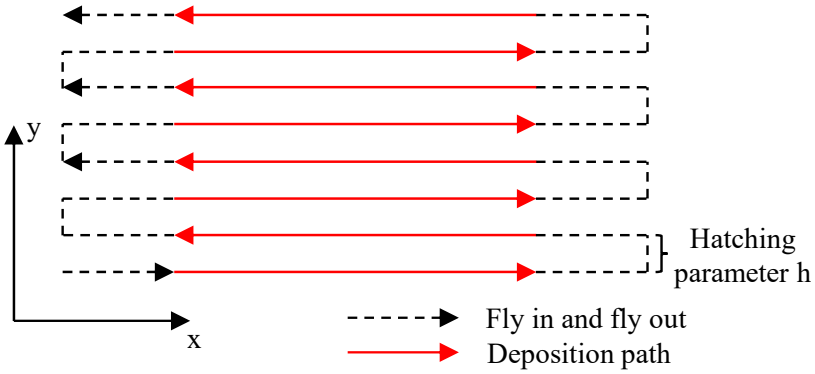

Figure 5. Path planning for the coating deposition.

Each coating area had a dimension of 30 mm × 30 mm and was analyzed via metallographic cross-sections (see Figure 6) for an average coating thickness measurement and evaluation of deposition defects. For the height measurement, five resulting thicknesses of the local maxima and local minima were measured within the microscopical image.

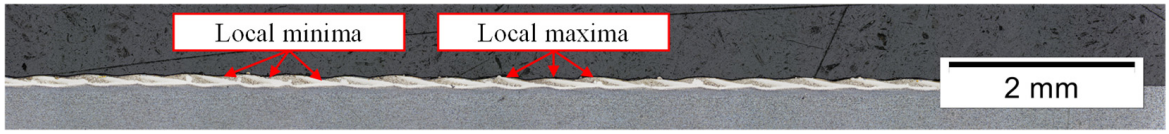

Figure 6. Metallographic cross-section of a coating specimen.

By incorporating a tilt/turn table, the EHLA3D technology enables the coating of free-form surfaces, which are neither planar nor rotationally symmetric, as the orientation of the processing optics can be flexibly set up perpendicular to the processing surface. However, depending on the geometry of the components, interfering contours can prevent the condition of a perpendicular deposition on the processing surface (see Figure 7a). To evaluate the process stability towards non-vertical surfaces, the developed coating parameter was applied on substrates with a variation of the tilting angle between 0° and 50°. The deposition was conducted parallel as well as perpendicular to the rotatory axis (see Figure 7b,c). The coating surfaces were qualitatively evaluated with a Keyence 3D optical profilometer VR-500 and metallographic cross-sections.

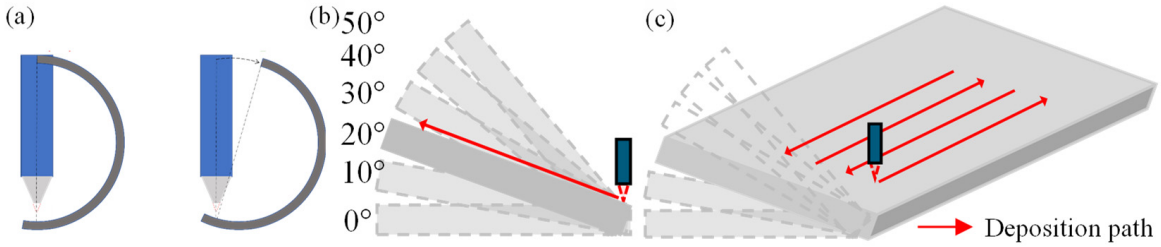

Figure 7. (**a**) Collision of processing optics with perpendicular deposition to the surface due to interfering contours. Experimental set-up for the evaluation of the tilted deposition, (**b**) perpendicular deposition to the rotatory axis, and (**c**) parallel deposition to the rotatory axis.

After the evaluation of the stability towards non-perpendicular deposition, a tilting range was proposed in which the EHLA3D process can be applied for a stable free-form coating.

2.3.3. Volume

To qualify the process for additive manufacturing and repair applications, the developed coating parameters from stage two were transferred to the deposition of bulk specimens in a third stage. Within the process transfer, the beam power was varied and the average coating layer thickness was defined as the initial Δz increment for the height adjustment per layer. The correct Δz increment with which the programmed height matched the actual built height was iteratively reduced and determined. For the bulk deposition, the cross-hatching path-planning strategy was applied (see Figure 8). The specimen geometry had dimensions of 30 mm × 30 mm (W × L) and 20 deposited layers for the high productivity and 60 layers for the low heat input parameter set.

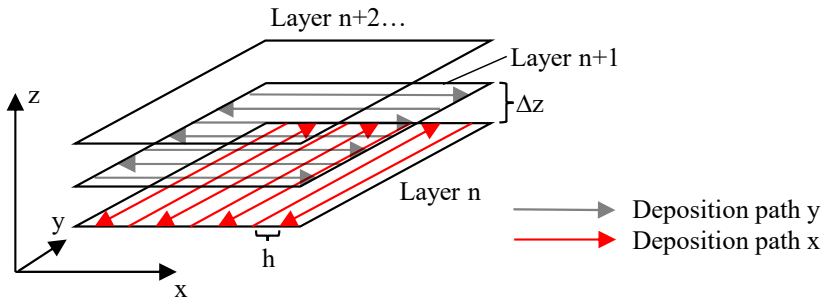

Figure 8. Path planning for bulk deposition with a cross-hatching strategy.

The deposited specimens were evaluated via metallographic cross-sections from which the proportion of porosity was measured (see Figure 9). A magnification of 6.3× was used for the porosity measurement. For this study, a porosity value of ≤0.5% (relative volume density of ≥99.5%) was defined as a target.

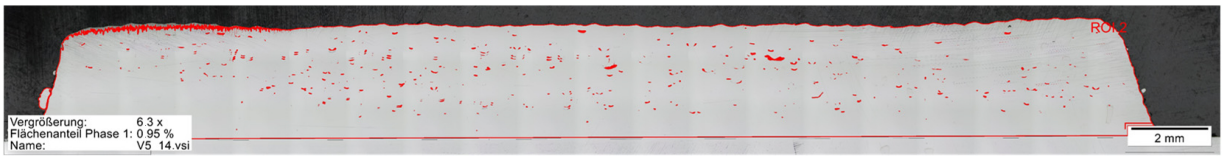

Figure 9. Metallographic cross-section of a bulk specimen with measurement of the porosity.

After the development and definition of the parameter set for (AM) deposition, a final specimen was deposited with target dimensions of 30 mm × 30 mm and a deposition height of ≥10 mm. In addition to the metallographic evaluation, the final probe was analyzed with SEM to identify micro defects. For the evaluation of the resulting material property, HV hardness measurements according to the DIN EN ISO14577 and DIN EN ISO 6507

with a test load of 300 g were conducted on the final probe specimen. In the scope of the hardness test, the point of indentation was placed on a line over the deposition height (see Figure 10) so that a hardness profile could be measured.

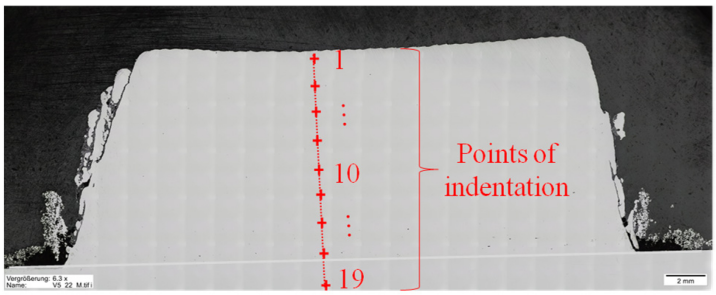

Figure 10. Points of indentation for the HV hardness measurement.

3. Results and Discussion

3.1. Single Track

For the evaluation of the influence of the process parameters on the deposition quality, a parameter study was conducted via deposition of single tracks and variation in the process parameters. The dependency between the investigated beam diameter and the resulting single-track geometries is presented in Figure 11.

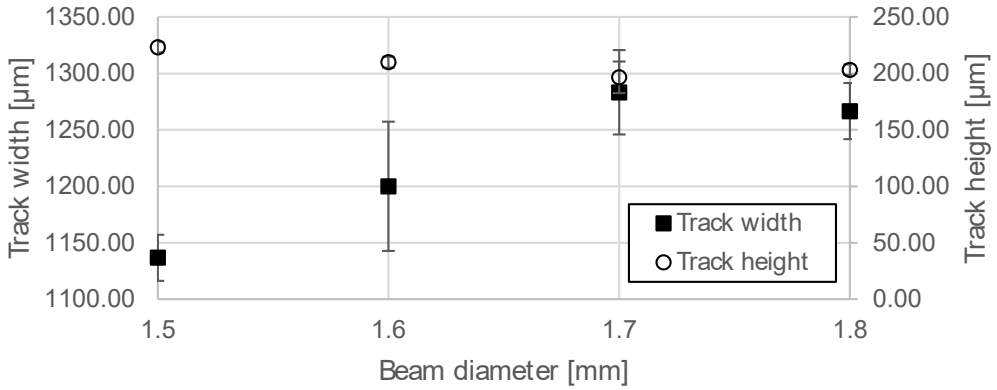

Figure 11. Influence of the beam diameter on the deposited single-track width and heigh. P_L = 2800 W; $\dot{m}$ = 2.2 kg/h; and Q_L = 8 L/min.

The beam diameter directly influences the resulting track width as the melt pool dimension is directly affected by the beam diameter. However, the resulting track width and melt pool dimension is ~400 µm smaller than the beam diameter used. The applied energy density distribution is a gaussian-like profile which has a high peak in the center and steeply decreases towards the beam diameter, which results in a smaller track width and a convergence towards a ~1270 µm track width. While the beam diameter directly affects the resulting track width, the track height is nearly unaffected at ~200 µm. The resulting single-track height is mainly influenced by the set powder mass flow (see Figure 12).

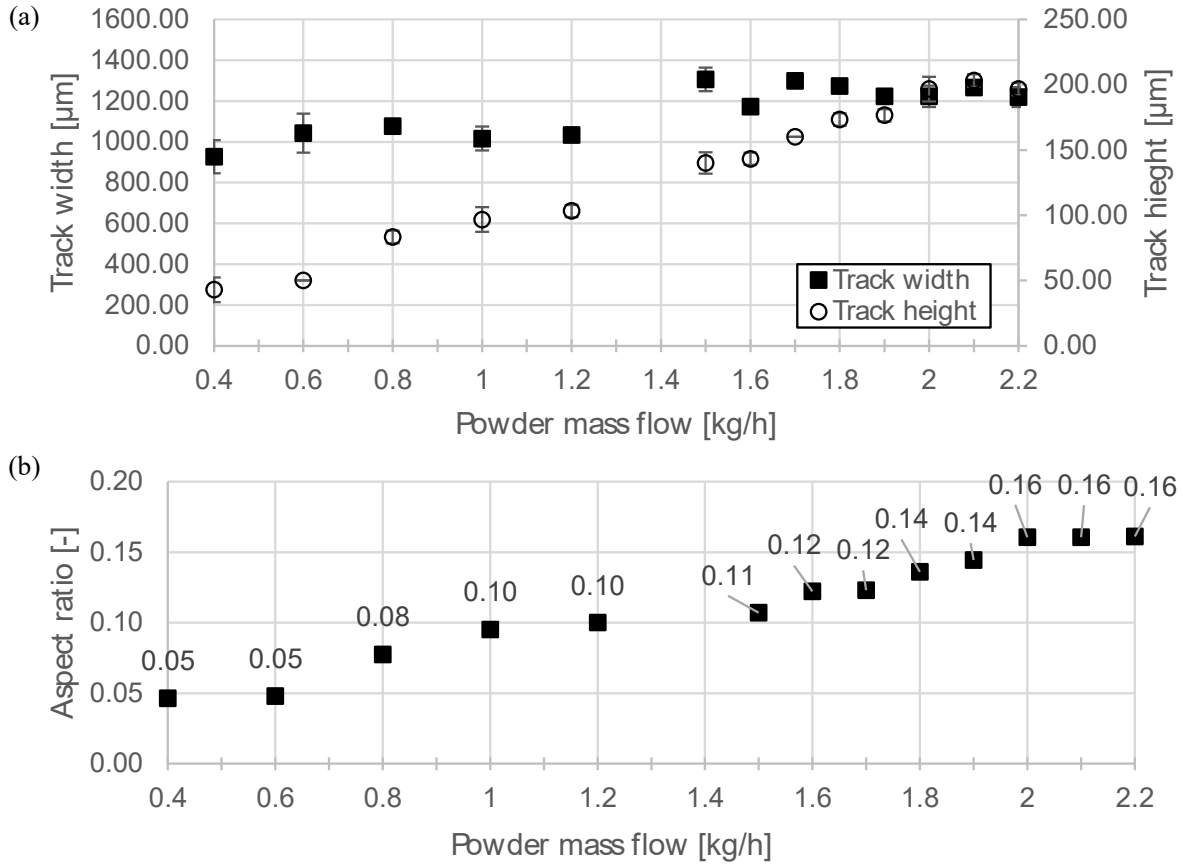

Figure 12. Resulting single-track geometries at different powder mass flows: (**a**) single track width and height (**b**) aspect ratios. d_B = 1.6 mm; Q_L = 8 L/min; P_L = 2000 W for 0.4 kg/h < ṁ < 1.2 kg/h; and P_L = 2600 W for 1.5 kg/h < ṁ < 2.2 kg/h.

An increasing powder mass flow results in an increasing single-track height towards ~200 µm at ṁ = 1.9 kg/h while the single-track width is not greatly affected. The single-track width stays nearly constant at either ~1000 µm for ṁ < 1.2 kg/h or at 1200 µm for ṁ > 1.5 kg/h, indicating that a threshold of powder supply is required for a full single-track width distribution along the formed melt pool. As the single-track height stays nearly constant, the aspect ratio continuously increases with an increasing powder mass flow until an aspect ratio of A = 0.16.

Results of varying the beam power indicate that the single-track geometries are mostly unaffected by the beam power parameter (see Figure 13a). However, the beam power directly influences the formation of the dilution zone (see Figure 13b).

According to the results, the beam power is primarily used for the bonding mechanism between the weld bead via formation of a dilution zone. The dimension of the dilution zone also increases as the energy input increases with increasing beam power. Also, the dilution zone depth decreases with an increasing powder mass flow since a higher powder mass flow results in a higher powder particle density within the powder gas jet stream. Due to this, more powder particles can absorb the beam power so that a smaller proportion of the beam energy reaches the substrate surface. An additional parameter is the carrier gas flow Q_C which influences the track geometries and the formation and dimension of the dilution zone (see Figure 14).

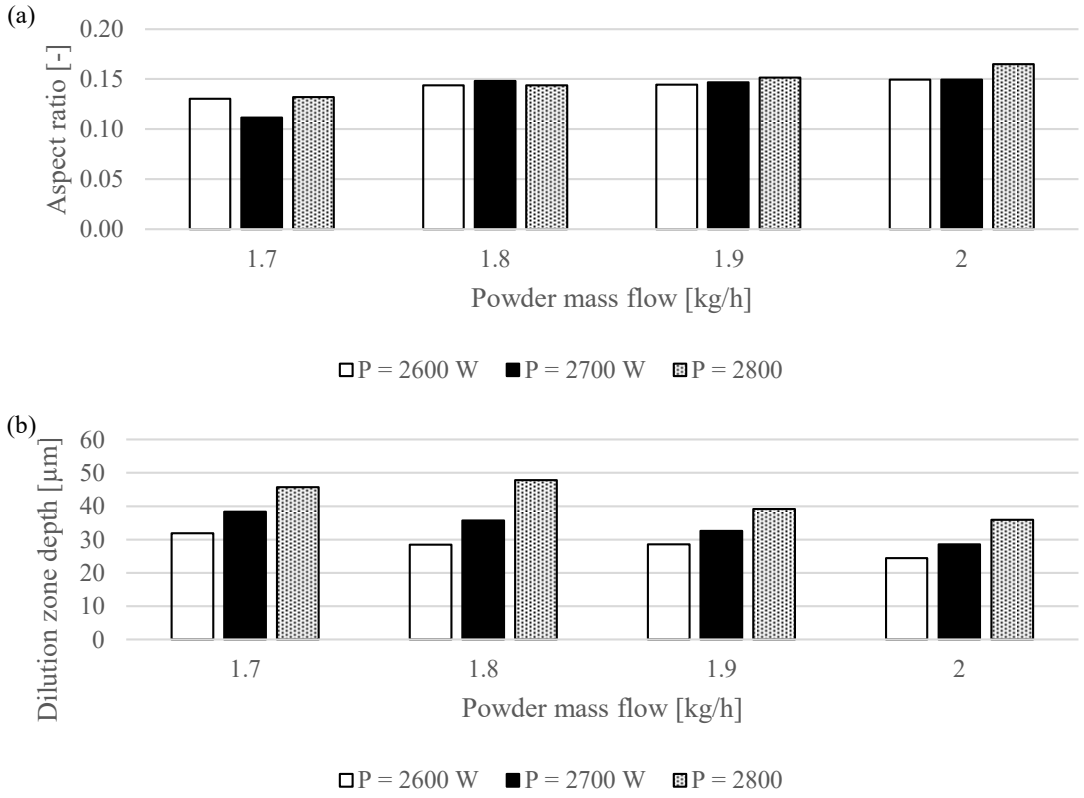

Figure 13. (**a**) Single-track aspect ratio and (**b**) dilution zone depth with variation in beam power. d_B = 1.6 mm and Q_L = 8 L/min.

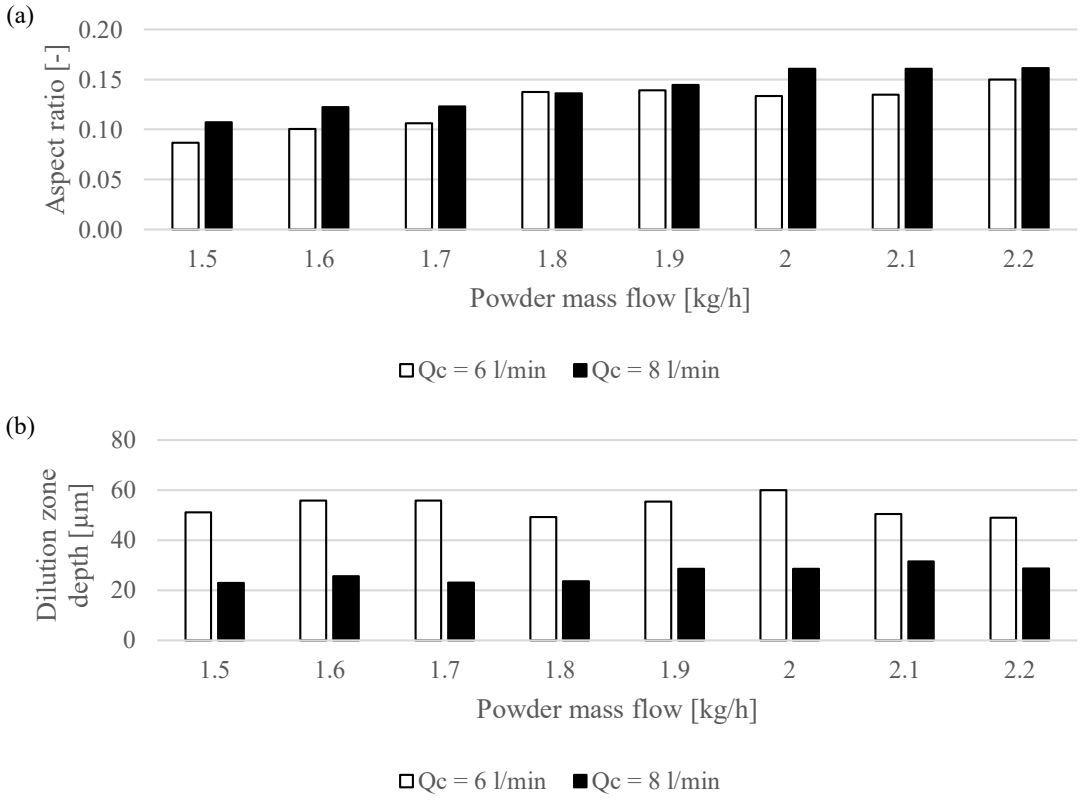

Figure 14. (**a**) Single-track aspect ratios and (**b**) dilution zone depths with variation in powder mass flow and carrier gas flows. d_B = 1.6 mm; P_L = 2600 W.

Similar to the variation in powder mass flows (see Figure 12), an increase in the carrier gas flow results in an increase in the deposited single-track height while the width is not greatly affected. Due to this, the single-track aspect ratio is also increasing with a higher carrier gas flow. This can be explained by a higher powder particle velocity which decreases the interaction time of the particle in the laser beam, so that less heat input is generated into the process. This results in a decrease in the dilution zone depth by ~50% by increasing the carrier gas flow from Q_C = 6 L/min to Q_C = 8 L/min. As less powder material can be incorporated into the dilution zone area, the single-track height is increased.

As the conclusion of the single-track study, the process parameters, which were selected for the transfer to a coating process, are presented in Table 3.

Table 3. Selected process parameter sets for the coating deposition and the resulting single-track properties.

Parameter set: high productivity	P_L [W]	$\dot{m}$ [kg/h]	Q_C [L/min]	d_B [mm]	V_f [m/min]
	2800	1.9	8	1.6	30
Single-track cross-section					
Single-track properties	Width [µm]	Height [µm]	Aspect ratio [-]		Dilution zone depth [µm]
	1223 ± 26	176 ± 5	0.14		28.6
Parameter set: Low heat input	P_L [W]	$\dot{m}$ [kg/h]	Q_C [L/min]	d_B [mm]	V_f [m/min]
	2000	0.4	8	1.6	30
Single-track cross-section	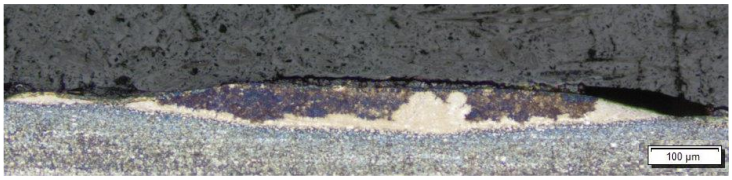				
Single-track properties	Width [µm]	Height [µm]	Aspect ratio [-]		Dilution zone depth [µm]
	927 ± 80	43 ± 9	0.05		39.0

3.2. Coating

The selected process parameters of the single-track parameter study were applied for a coating process via the deposition of multiple, overlapping single-tracks. The overlap was set via the hatch distance parameter h, which has an influence on the resulting coating thickness (see Figure 15).

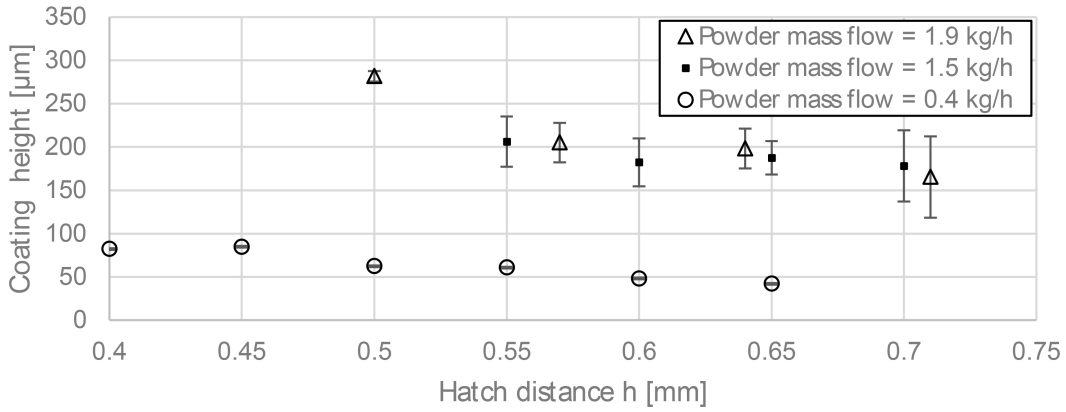

Figure 15. Resulting coating thicknesses by variation in the hatching distance h. Applied parameter sets are provided in Table 3.

The resulting coating thickness can be deposited in a range between 60 µm and 281 µm depending on which parameter sets and hatch distance are applied. The coating thickness increases with decreasing hatch distance as a higher proportion of the single-track overlaps with the next deposited single-track, which results in local material accumulation. In addition, the deviation decreases since the local minima approximates towards the maxima (see Figure 16).

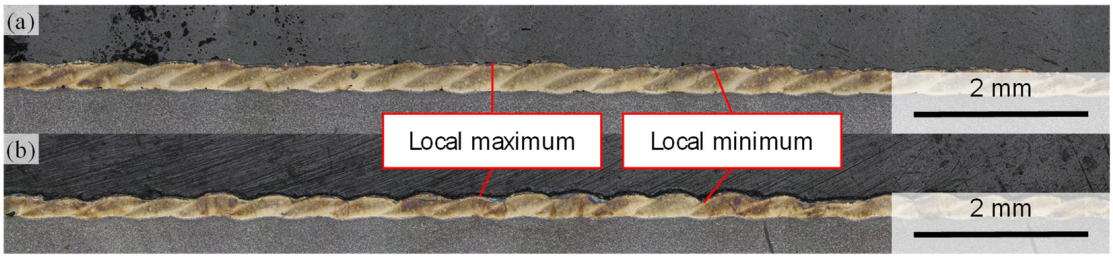

Figure 16. Metallographic cross-sections of coatings deposited with parameter set ṁ = 1.9 kg/h. (**a**) h = 0.5 and (**b**) h = 0.6.

By decreasing the hatching distance, a smoother coating surface with smaller thickness deviation can be achieved. However, bonding defects are incorporated when a low hatching distance is applied, since the prior deposited weld bead is not fully melted (see Figure 17).

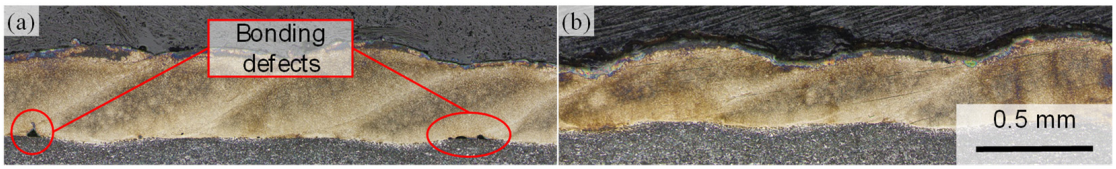

Figure 17. Bonding defects at the end of a weld track at a low hatch distance. (**a**) h = 0.5 and (**b**) h = 0.6 with the ṁ = 1.9 kg/h parameter set.

In the scope of the investigated parameters, the following process parameter sets for the single-layer coating deposition are defined, which result in a sufficient deposition quality with no bonding defects (see Table 4).

Table 4. Coating process parameters.

Parameter Set	P_L [W]	$\dot{m}$ [kg/h]	Q_C [L/min]	d_B [mm]	V_f [m/min]	h [mm]	Coating Thickness [µm]
High productivity	2800	1.9	8	1.6	30	0.6	205 ± 22
Low heat input	2000	0.4				0.55	60 ± 10

One major challenge of the free-form tool path planning can be the definition of tool paths with high feed-rates, which bear the high risk of tool collision. Due to this, interfering contours can prevent a perpendicular deposition on a free-form surface while an angled deposition can enable a coating process without tool collision (see Figure 7a). Single layers were deposited with the parameter set $\dot{m}$ = 0.4 kg/h at different deposition angles, parallel as well as perpendicular to the rotatory axis (see Figure 18), to investigate the feasibility of angled deposition.

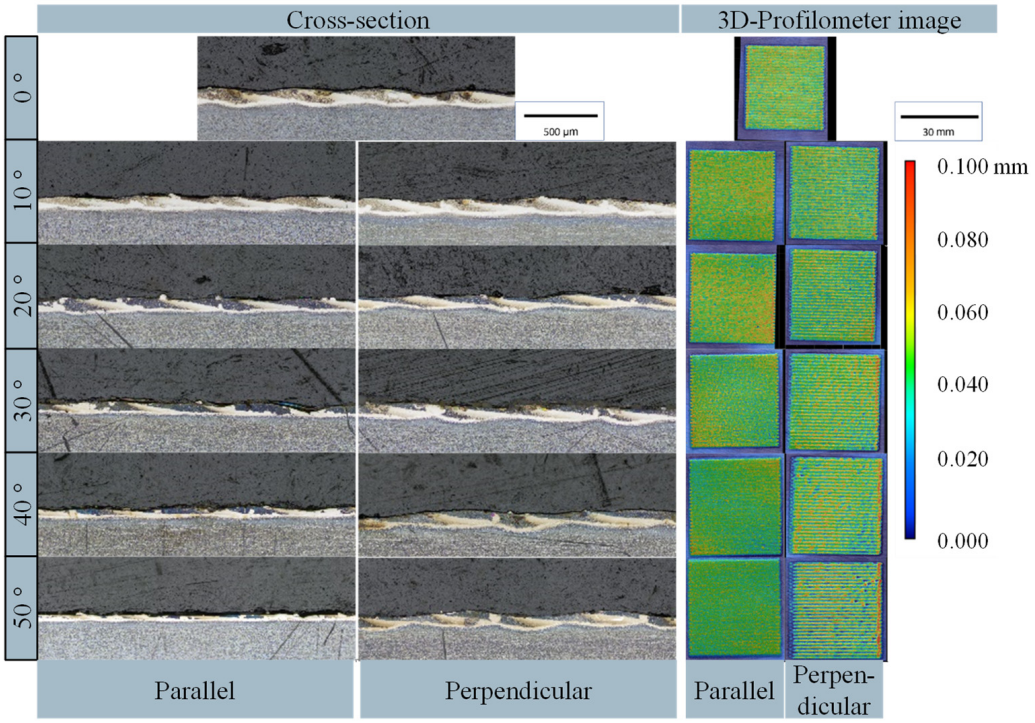

Figure 18. Metallographic cross-sections and 3D-profilometer images of probes deposited at different angles.

The cross-section as well as the topography of the layers deposited parallel and perpendicular to the rotation axis are qualitatively comparable until an angle of 20°. From 20° onwards, the height and the dilution zone of the parallel deposited layer decreases with an increasing angle. In the case of perpendicular deposition, the topographic image validates increasing irregularities of the tracks with increasing angle. This is also verified by the irregular layer height and dilution zone depths in the metallographic cross-section. According to the qualitative analysis, a feasible coating process can be expected up until an angled deposition of 20°.

3.3. Volume

In the last stage, the feasibility of the process parameters for additive manufacturing were investigated via deposition and stacking of layers with a Δz increment as an additional parameter. Initially, the resulting average single-layer thickness was applied as the Δz

increment. To deposit the targeted set height, the Δz increment needed to be iteratively reduced until the programmed set height matched the deposited specimen height. The resulting parameter sets with the corrected Δz increments are presented in Table 5.

Table 5. Process parameter sets for the deposition of bulk specimen.

Parameter Set	P_L [W]	$\dot{m}$ [kg/h]	Q_C [L/min]	d_B [mm]	V_f [m/min]	h [mm]	Δz [µm]
High productivity	2800	1.9	8	1.6	30	0.6	190
Low heat input	2000	0.4				0.55	55

According to the metallographic cross-section of the bulk specimen, the deposition with the parameter set $\dot{m}$ = 1.9 kg/h results in an insufficient bonding to the substrate material, due to crack formations at the edge area of the specimen (see Figure 19).

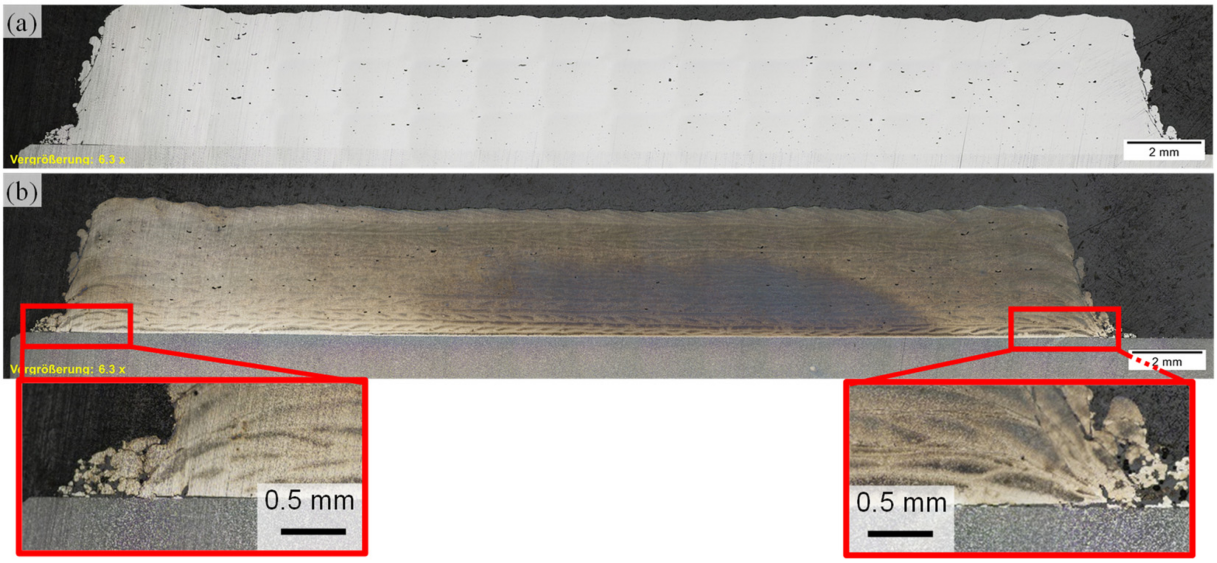

Figure 19. Metallographic cross-section of the bulk specimen deposited with the high productivity parameter set. (**a**) Polished cross-section and (**b**) etched cross-section—resulting porosity: 0.34%.

The crack formation most likely results from heat-induced stresses built up during the deposition process. A porosity of 0.34% can be achieved; however, due to the crack formation as a critical defect, the parameter set cannot be applied for additive manufacturing. As the parameter set with $\dot{m}$ = 0.4 kg/h operates with a lower beam power, bulk specimens were deposited without crack formation. However, beam power adaptions were required to reduce the porosity from 1.23% to 0.11% (see Table 6).

The variation in the beam power verifies that, initially, a too-high beam power was applied for the deposition of bulk specimen. The porosity formation at the set beam power > 1600 W can be explained by either local material evaporation or a lower melt pool viscosity resulting in a turbulent flow, in which the liquid material solidifies around hollow space. To investigate further the feasibility of the identified parameter set for additive manufacturing, a specimen with 250 layers was deposited and analyzed via metallography and SEM (see Figure 20).

Table 6. Influence of beam power on porosity for the deposition of bulk specimen. v_f = 30 m/min; d_B = 1.6 mm; $\dot{m}$ = 0.4 kg/h; Q_C = 8 L/min; h = 0.55 mm; and Δz = 55 µm.

P_L [W]	Metallographic Cross-Section	Porosity [%]
2100	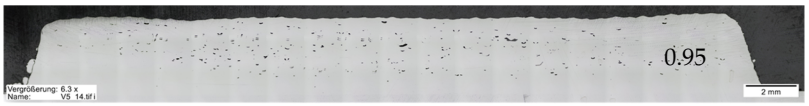	0.95
2000	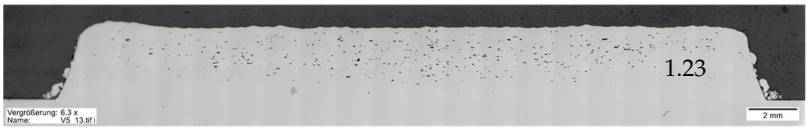	1.23
1800		0.68
1600		0.11

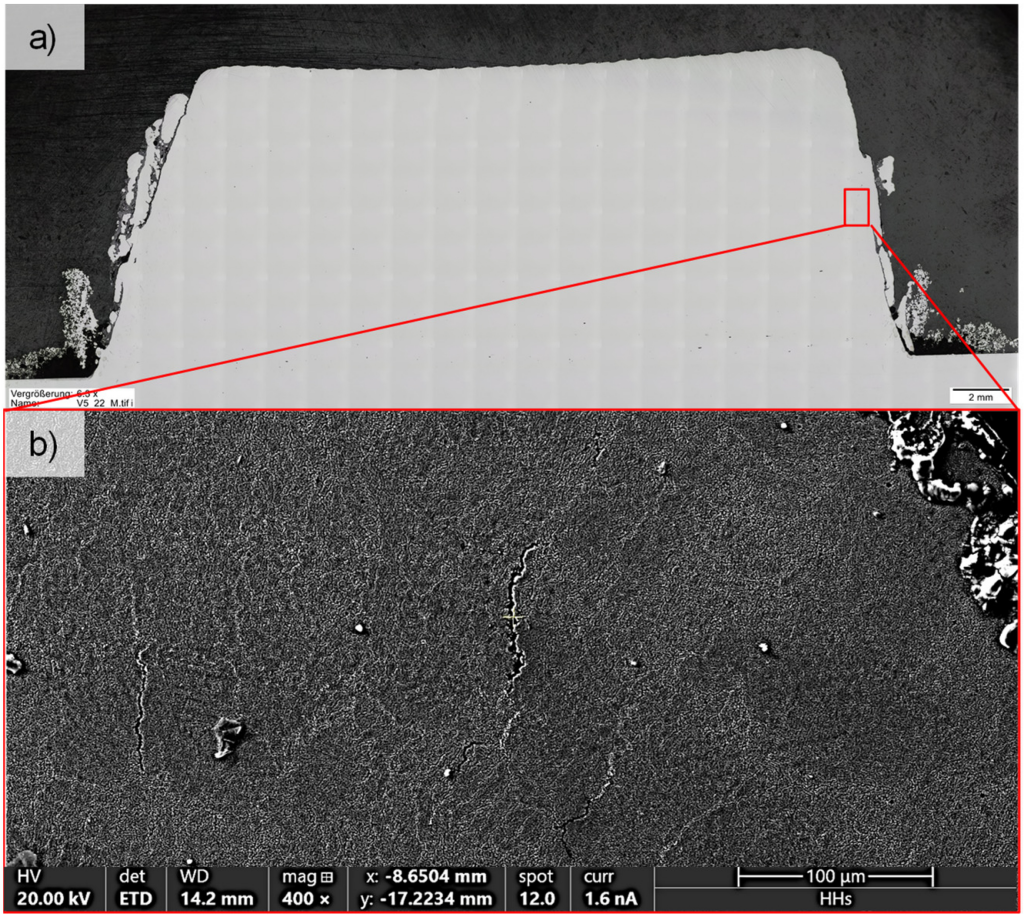

Figure 20. (**a**) Metallographic cross-section of a bulk specimen with 250 deposited layers—porosity: 0.04 %. (**b**) SEM image of the edge area with identified micro hot cracks.

The metallographic analysis validates a porosity of 0.04% and the largest identified pore dimension of 109 µm, further proving that the parameter set can be potentially applied

for the deposition of bulk geometries. However, thermal induced micro hot cracks are identified via SEM images. The micro cracks, which did not appear in the specimens with lower volumes, occur in the edge region within ~1 mm from the edge so that the inner part of the specimen is defect free. Hence, when depositing larger volumes with the parameter set, the micro cracks need to be removed within a subtractive post processing. For the final evaluation, the hardness values of the specimen were measured (see Figure 21).

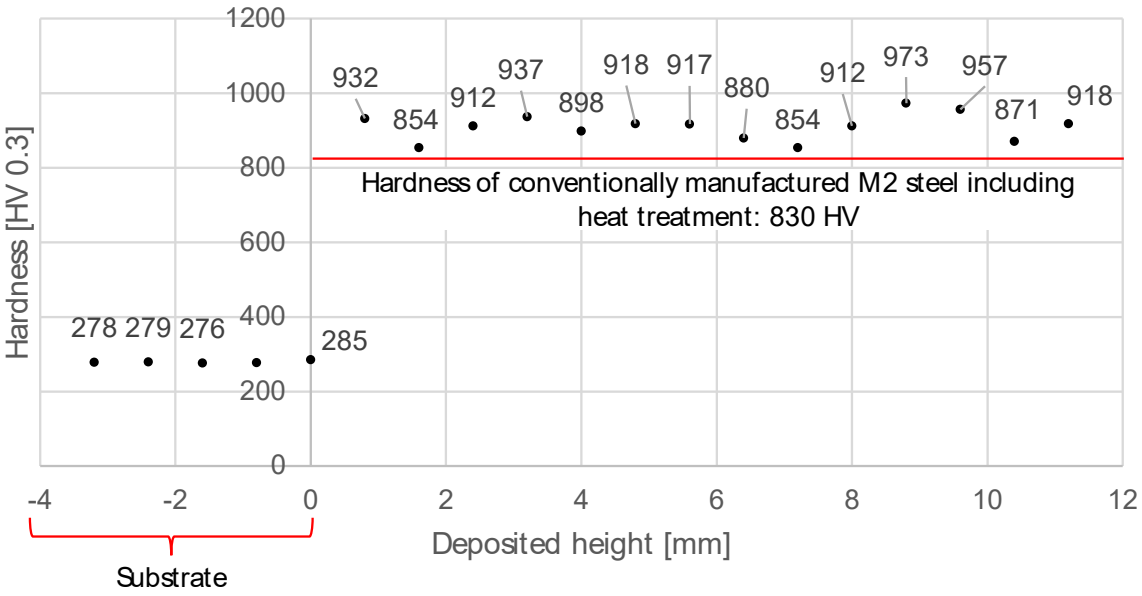

Figure 21. Hardness profile of the deposited bulk specimen—average hardness: 910 ± 34 HV.

The resulting hardness of the as-built specimen is 910 ± 34 HV (≈67.5 HRC) which exceeds conventionally manufactured M2 parts of 830 HV after a heat treatment process. As such, similar to the M2 deposition with conventional DED, a heat treatment is not required, as the thermal conditions during the deposition and cooling result in a microstructure with sufficient hardness properties.

4. Conclusions

4.1. Single Track

In the scope of this work, a EHLA3D process parameter study with the material M2 was conducted by evaluating the influence of the process parameters on the deposition of a single track. Within the conducted parameter variations, the following key results can be summarized for the single-track parameter study:

- Weld bead geometry: the resulting weld bead width is mainly influenced by the set beam diameter while the powder mass flow mainly affects the resulting single-track height. An increasing carrier gas flow also results in a small increase in the single-track height. The beam power only has a minor effect on the resulting single-track geometry;
- Dilution zone: an increasing beam power results in an increasing dilution zone depth. Also, a major parameter which affects the dilution zone is the carrier gas flow because this parameter affects the interaction time between powder particle and laser beam in the EHLA process. Hence, the bonding to the substrate material as well as the generated heat input into the substrate can be controlled with the beam power and carrier gas flow.

4.2. Coating

After the single-track parameter study, a single-layer coating parameter was developed by investigating the effect of the hatching parameter on the resulting coating thickness.

- The resulting coating thickness increases with a decreasing hatching parameter as a higher proportion of the prior deposited weld bead overlaps with the next deposited weld bead. The deviation of the coating thickness can be reduced with a decreasing hatching parameter; however, lack of bonding begins to occur at small hatching parameter within this study;
- Coating parameters with a set powder mass flow of $\dot{m}$ = 1.9 kg/h and $\dot{m}$ = 0.4 kg/h were developed and result in an average coating thickness of 205 µm and 60 µm, respectively. Compared to the parameters provided in the literature, the powder mass flow is increased by 0.1 kg/h when applying the parameter set with a lower heat input. In the case of the parameter set with $\dot{m}$ = 1.9 kg/h, the powder mass flow is increased by 1.6 kg/h;
- The experiments with non-perpendicular deposition qualitatively indicate that the coating process tolerates a tilting angle of up to 20°. This can be potentially applied when a perpendicular deposition condition is not applicable due to interfering contours of a component.

4.3. Volume

The developed coating parameters were also investigated towards the application of additive manufacturing via deposition of multiple layers with an Δz adjustment between each layer:

- Due to high thermal-induced stresses, which lead to crack formation in the bonding zone, the parameter set with $\dot{m}$ = 1.9 kg/h cannot be applied for the deposition of bulk specimens. A variation in deposited geometries, which potentially prevents a crack formation, can be further investigated in following experiments;
- Due to a lower generated heat input, a parameter set for additive manufacturing could be developed with the set powder mass flow of $\dot{m}$ = 0.4 kg/h. However, the formation of micro cracks is identified at the area within 1 mm from the specimen edge, when bigger volumes are deposited. The micro defects need to be potentially removed in post-processing steps;
- The conducted hardness measurements on the bulk specimen validate that a hardness of ~900 HV can be achieved without heat treatment. As a conclusion, when post-processing steps are considered, the developed process parameter can be applied for the additive manufacturing of simple geometries or repair applications. To further investigate the feasibility of depositing more complex structures and geometries, future studies need to be extended with the deposition of different geometrical features.

Author Contributions: Conceptualization, M.-U.K. and J.C.; methodology, M.-U.K. and J.C; validation, M.-U.K.; formal analysis, M.-U.K.; investigation, J.C.; data curation, M.-U.K. and J.C; writing—original draft preparation, M.-U.K.; writing—review and editing, M.-U.K. and T.S.; visualization, M.-U.K.; supervision, T.S. and C.H.; project administration, M.-U.K. All authors have read and agreed to the published version of the manuscript.

Funding: The authors declare that this study received funding from Makino Asia Pte Ltd., Singapore. The funder had the following involvement with the study: development and provision of the EHLA3D machine used in this work.

Institutional Review Board Statement: Not applicable.

Informed Consent Statement: Not applicable.

Data Availability Statement: Data is contained within the article.

Conflicts of Interest: Author Julius Cüppers was employed by the company Makino Asia Pte Ltd. The remaining authors declare that the research was conducted in the absence of any commercial or financial relationships that could be construed as a potential conflict of interest.

References

1. Kelbassa, I. Qualifizieren des Laserstrahl-Auftragschweißens von BLISKs aus Nickel- und Titanbasislegierungen. Ph.D. Thesis, Faculty of Mechanical Engineering, Aachen, Germany, 2006.
2. Witzel, J. Qualifizierung des Laserstrahl-Auftragschweißens zur generativen Fertigung von Luftfahrtkomponenten. Ph.D. Thesis, Faculty of Mechanical Engineering, Aachen, Germany, 2015.
3. Baek, G.Y.; Shin, G.Y.; Lee, E.M.; Shim, D.S.; Lee, K.Y.; Yoon, H.S.; Kim, M.H. Mechanical Characteristics of a Tool Steel Layer Deposited by Using Direct Energy Deposition. *Met. Mater. Int.* **2017**, *23*, 770–777. [CrossRef]
4. Park, Y.K.; Ha, K.; Shin, K.Y.; Lee, K.Y.; Kim, D.J.; Kwon, S.H.; Lee, W. Wear resistance of direct-energy–deposited AISI M2 tool steel with and without post-heat treatment. *Int. J. Adv. Manuf. Technol.* **2021**, *16*, 3917–3931. [CrossRef]
5. Svetlizky, D.; Zheng, B.; Vyatskikh, A.; Das, M.; Bose, S.; Bandyopadhyay, A.; Schoenung, J.M.; Lavernia, E.J.; Eliaz, N. Laser-based directed energy deposition (DED-LB) of advanced materials. *Mater. Sci. Eng. A* **2022**, *840*, 142967. [CrossRef]
6. Bajaj, P.; Hariharan, A.; Kini, A.; Kürnsteiner, P.; Raabe, D.; Jägle, E.A. Steels in additive manufacturing: A review of their microstructure and properties. *Mater. Sci. Eng. A* **2020**, *772*, 138633. [CrossRef]
7. Li, Y.; Wang, Y.; Niu, J.; Liu, S.; Lin, Y.; Liu, N.; Ma, J.; Zhang, Z.; Wang, J. Microstructure and mechanical properties of M2 high speed steel produced by electron beam melting. *Mater. Sci. Eng. A* **2023**, *862*, 144327. [CrossRef]
8. Chaus, A.S.; Bračík, M.; Sahul, M.; Dománková, M. Microstructure and properties of M2 high-speed steel cast by the gravity and vacuum investment casting. *Vacuum* **2019**, *162*, 183–198. [CrossRef]
9. Otai Special Steel M2 Tool Steel | 1.3343 | HS-6-5-2C | SKH51. Available online: https://www.astmsteel.com/product/m2-tool-steel-1-3343-hs-6-5-2c-skh51/ (accessed on 13 May 2024).
10. Moritz, S.; Schwanekamp, T.; Reuber, M.; Lentz, J.; Boes, J.; Weber, S. Impact of in Situ Heat Treatment Effects during Laser-Based Powder Bed Fusion of 1.3343 High-Speed Steel with Preheating Temperatures up to 700 °C. *Steel Res. Int.* **2023**, *94*, 2200775. [CrossRef]
11. Schopphoven, T. Experimentelle und modelltheoretische Untersuchungen zum Extremen Hochgeschwindigkeits- Laserauftragschweißen. Ph.D. Thesis, Faculty of Mechanical Engineering, Aachen, Germany, 2019.
12. Xu, X.; Lu, H.; Qiu, J.; Luo, K.; Su, Y.; Xing, F.; Lu, J. High-speed-rate direct energy deposition of Fe-based stainless steel: Process optimization, microstructural features, corrosion and wear resistance. *J. Manuf. Process.* **2022**, *75*, 243–258. [CrossRef]
13. Yong, Z.; Chang, L.; Jiang, S.; Xie, D.; Xing, F.; Shen, H.; Shen, L.; Tian, Z. Parameter optimization of T800 coating fabricated by EHLA based on response surface methodology. *Opt. Laser Technol.* **2023**, *158*, 108837. [CrossRef]
14. Meghwal, A.; Pinches, S.; Anupam, A.; Lie, L.; Munroe, P.; Berndt, C.C.; Ang, A.S.M. Structure-property correlation of a CoCrFeNi medium-entropy alloy manufactured using extreme high-speed laser material deposition (EHLA). *Intermetallics* **2023**, *152*, 107769. [CrossRef]
15. TRUMPF SE + Co. KG. Laser Metal Deposition—A Process for Various Applications. Available online: https://www.trumpf.com/en_INT/solutions/applications/additive-manufacturing/laser-metal-deposition/ (accessed on 4 June 2024).
16. ponticon GmbH. Coating, Repair and Additive Manufacturing in Three Dimensions. Available online: https://ponticon.de/en/produkte/ (accessed on 4 June 2024).
17. Bold, M.-N.; Schleifenbaum, J.H.; Schmitt, N. *Application of the 3D-EHLA Process for Agile Alloy Development*; Universitätsbibliothek der RWTH Aachen: Aachen, Germany, 2022.
18. Makino Asia Pte Ltd. AML500 5-Axis CNC Machine for High-Speed DED. Available online: https://www.makino.com.sg/en-us/machine-technology/machines/laser-metal-deposition/aml500 (accessed on 3 January 2024).
19. Schaible, J.; Sayk, L.; Schopphoven, T.; Schleifenbaum, J.H.; Häfner, C. Development of a high-speed laser material deposition process for additive manufacturing. *J. Laser Appl.* **2021**, *33*, 012021. [CrossRef]
20. Ko, M.-U.; Zhang, Z.; Schopphoven, T. Process development and process adaption guidelines for the deposition of thin-walled structures with IN718 using extreme high-speed directed energy deposition (EHLA3D). *J. Laser Appl.* **2023**, *35*, 042059. [CrossRef]